# Final results from MCF-experiments in $D_2$ and HD gases

N.I. Voropaev [a], D.V. Balin [a], W.H Breunlich [b], T. Case [c], K.M. Crowe [c], M.P. Faifman [e], B. Gartner [b], F.J. Hartmann [d], P. Kammel [c], B. Lauss [b], E.M. Maev [a], V.E. Markushin [f], C. Petitjean [f], G.E. Petrov [a], G.N. Schapkin [a], G.G. Semenchuk [a], A.A. Vorobyov [a], J. Zmeskal [b]

[a] *Petersburg Nuclear Physics Institute (PNPI), Gatchina 188350, Russia*
[b] *Institute for Medium Energy Physics (IMEP), A-1090 Wien, Austria*
[c] *University of California Berkeley, UCB and LBNL, Berkeley, CA 94720, USA*
[d] *Technical University of Munich (TUM), D-85747 Garching, Germany*
[e] *Russian Research Centre "Kurchatov Institute", Moscow 123182, Russia*
[f] *Paul Scherrer Institute, PSI, CH-5232 Villigen, Switzerland*

During 1994-1996, a series of $\mu$CF experiments was performed at PSI by the PSI-PNPI-IMEP-LBNL-TUM collaboration. These experiments aimed at high precision studies of the d-$\mu$-d fusion in $D_2$ and HD gases in a wide temperature range. The Gatchina ionization time projection chamber has been used to detect the dd-fusion reaction products. The main parameters of the d-$\mu$-d fusion have been measured with high absolute precision. In this report, we present the results of the final analysis of the experimental data. The obtained results are compared with the calculations based on a recent $\mu$CF-theory.

## 1. Introduction

After experimental discovery of resonant mechanism of dd$\mu$ molecule formation [1], due to the "Vesman mechanism" [2], muon catalyzed dd - fusion was the subject of numerous investigations, see reviews [3,4]. The agreement reached with the theory was quite impressive [5], still the method using the high pressure ionization chamber from Gatchina allows to investigate and test a number of dd$\mu$ problems on a qualitatively new level of accuracy $\sim 1\%$. This experimental method was described in [6–9] and was presented at this meeting also. Here we shall point out only the main features of the method. The high pressure hydrogen ionization chamber (IC) was used as an active target. It allowed to determine clean muon stops in the sensitive IC volume, well separated in space from the IC electrodes. The IC has the capability to detect with 100% efficiency all charged products of the dd-fusion reaction and to separate all the channels of this reaction

$$dd\mu \rightarrow \begin{cases} {}^3\mathrm{He}{+}\mathrm{n} + \mu \\ {}^3\mathrm{He}\mu + \mathrm{n} \\ \mathrm{t}{+}\mathrm{p} + \mu \ . \end{cases}$$

We have measured the d-$\mu$-d fusion observables with an absolute precision up to 1%. The IC could operate in a wide temperature range from 28K to 350K, the temperature being determined in each measuring point to absolute precision of ±0.15K. The IC was filled with pure $D_2$ or with $H_2$+$D_2$ gas mixture. Also, measurements were performed with a specially prepared pure HD gas where admixture of $D_2$ molecules was only on a level of 1%. The IC was surrounded with an array of scintillator counters for detection of neutrons from the fusion reaction. The main (though small) background in these studies was due to muon capture on the hydrogen contamination with $N_2$, $O_2$, $H_2O$ on a level a few ppm. However, the IC allowed to detect directly the products of the muon capture reactions and to subtract this background in the analysis of the experimental data. Preliminary results of these measurements were published in [10–12].

## 2. Analysis and Results

Below we present the results of analysis of the experimental runs performed at various temperatures with pure $D_2$ gas (17 runs), with equilibrated $H_2$+HD+$D_2$ (4 runs) and non-equilibrated $H_2$+$D_2$ (3 runs) gas mixture, and also with HD gas (3 runs).

For analysis, only those events were selected with the muon stops in the sensitive volume of the IC, well separated in space from the IC electrodes and from the walls. This selection was done using the amplitude and time distributions of the muon signals in the IC. Typically, around $10^6$ clean muon stops were selected in each run, and amplitude and time distributions of the fusion signals were analyzed. As an example, Fig.1 presents such distributions measured in pure $D_2$ at 120.3K. In the amplitude spectrum, one can see the peaks corresponding to the dd-fusion channels with $^3$He+n, $^3$He$\mu$+n, and t+p in the final state. The separation of the $^3$He and $^3$He$\mu$ peaks is due to difference in recombination of the primary ionization produced by the $^3\mathrm{He}^{++}$ and $^3\mathrm{He}\mu^+$ particles (initial energy around 0.8 MeV). The continuous spectrum of the t+p channel is a result of the probability for the long range protons ($E_p$ = 3.02 MeV) to escape from

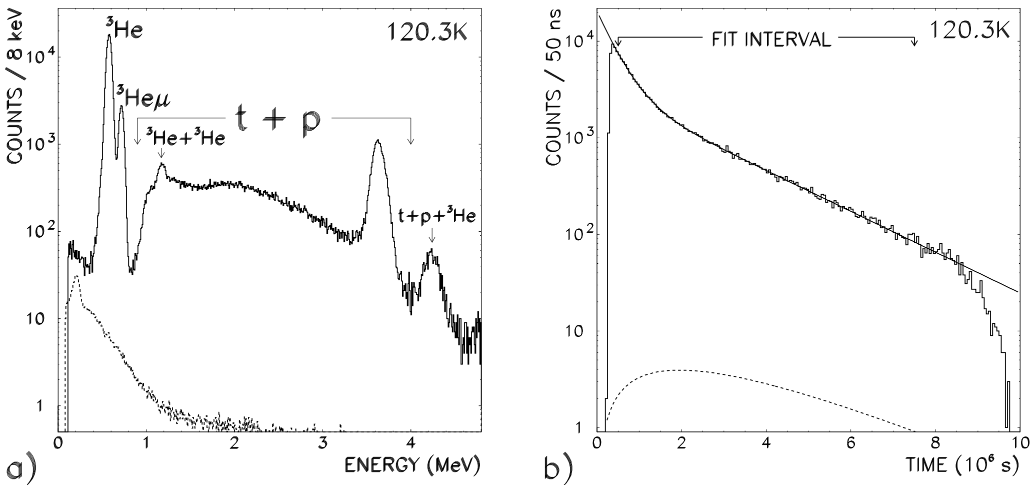


Figure 1. a) Amplitude spectrum of fusion signals from the IC in $D_2$ gas. The dashed line corresponds to muon capture background. b) Time distribution of $^3$He and $^3$He$\mu$ signals. The dashed line corresponds to the $\mu$-capture background. Solid line is the result of the kinetics fit.

the sensitive volume of the IC. The time distribution exhibits a typical two-exponential decay. The fast component is determined by the dd$\mu$ formation from the upper 3/2-state of the d$\mu$-atom. The slow component corresponds to the thermal steady equilibrium state between the lower and the upper states of the d$\mu$-atom where the dd$\mu$ formation occurs predominantly from the lower 1/2-state. The steady state amplitude distribution is shown in Fig.2a.

Analysis of the experimental data was performed using the kinetics scheme shown in Fig.2b. In a first step the background was subtracted consisting mainly from muon capture reactions on gas impurities (mostly $N_2$). A special run was carried out with a $H_2$+$N_2$(140 ppm) gas mixture, allowing to measure the amplitude distribution of the $\mu$-capture events. The time distribution of the $\mu$-capture events $Y_c$(t) was measured in a $D_2$ run at 50.2 K which contained the highest level of impurities. In these measurements, an amplitude interval $(0.1 \div 0.45)$ MeV was selected, where the $\mu$-capture events dominate. The measured $Y_c$(t) distribution allowed to determine the muon transfer rate to heavy admixture $\Lambda_Z$ and the detection efficiency for the $\mu$-capture events $w_r = 0.55(3)$. In addition, the muon capture rate was found to be: $\lambda_c = 0.057(6)$ $\mu s^{-1}$ that turned out to be equal to the known value of the $\mu$-capture rate on Nitrogen. It was possible to determine the $\mu$-capture background in each run by normalizing the $\mu$-capture

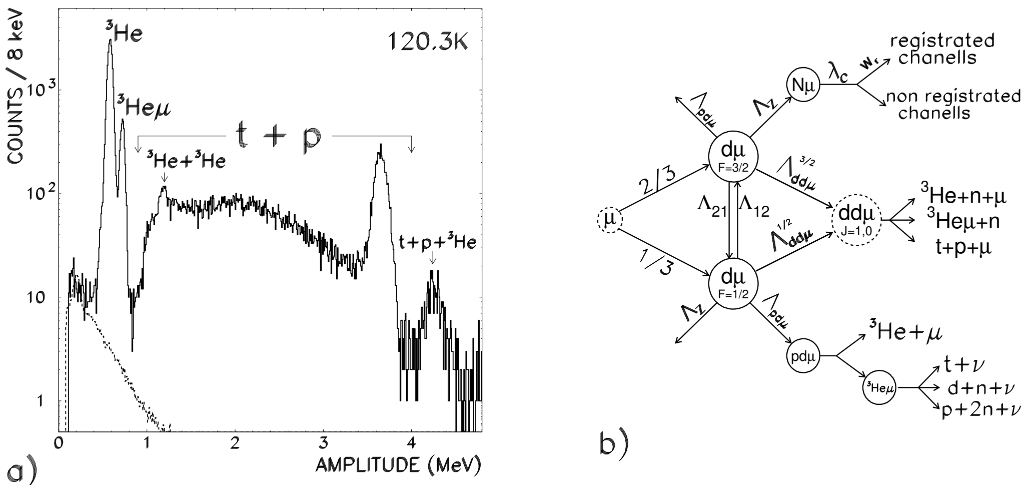


Figure 2. a) Amplitude spectrum of dd-fusion signals for steady-state time region ($t > 2\mu$s). b) Scheme of $\mu$CF kinetics used for data analysis.

amplitude distribution to the d-$\mu$-d fusion ones in the region $(0.1 \div 0.45)$ MeV, where $\mu$-capture events dominates (Fig.2a). Note that the steady-state region was used for this fit to exclude distortion of the low-energy part of the spectrum by signals of double muons (Fig.1a). Such normalization, together with the measured values for $\lambda_c$ and $w_r$, allowed to determine the transfer rate $\Lambda_Z = \lambda_Z \cdot C_Z \cdot \phi$ in each temperature point and, using the known value $\lambda_Z = 5 \cdot 10^{10}$ s$^{-1}$, to find the impurity concentration $C_Z$. Both values are presented in Tables $1 \div 3$. In the particular case of $D_2$ at 120.3 K, $C_Z$=1 ppm the $\mu$-capture background was very small (see Fig.1a and Fig.1b). It became more important for higher levels of impurities and for lower dd-fusion rates. However, in all cases this capture background was under control and could not deteriorate the analysis precision. Other sources of background (double muon events, etc.) were negligible. This was checked in a run with $\mu^+$ beam.

### *2.1. dd$\mu$ - molecule formation and spin-flip processes*

From the analysis of the time distributions of the first $^3$He and $^3$He$\mu$ signals (Fig.1b), one can determine the dd$\mu$-molecule formation rates $\Lambda^{3/2}_{dd\mu} = \lambda^{3/2}_{dd\mu} \cdot C_d \cdot \phi$ and $\Lambda^{1/2}_{dd\mu} = \lambda^{1/2}_{dd\mu} \cdot C_d \cdot \phi$ from the F=3/2 and F=1/2 hyperfine states, respectively, and also the transfer rate $\Lambda_{21} = \lambda_{21} \cdot C_d \cdot \phi$ from the F=3/2 to F=1/2 $d\mu$-states.

Here, $\phi$ is the normalized gas density, and $\lambda_{21}, \lambda^{3/2}_{dd\mu}, \lambda^{1/2}_{dd\mu}$ are the rates normalized to LHD ($\phi = 1$), $C_d$ is the deuterium atomic concentration. The time distribution of the $^3$He events was chosen for the following reasons:

1. The short tracks of the $^3$He particles lead to minimal dead time and smearing.

2. Pileup probabilities of a next fusion signal on muon signal or on $^3$He one are similar (because the same pulse durations), therefore the ratio $N(^3He)/N_\mu$ is measured without distortion.

3. There is possibility of precise ($\pm$1ns) measurement of actual beginning (t=0) of experimental $^3$He time distributions from the analysis of the time distributions of the dd-fusion neutrons detected by the scintillation counter array in coincidence with the $^3$He IC signals.

For quantitative analysis, the kinetics scheme in Fig.2b was used, and the following analytical solution for the time distribution of the first $^3$He signals was applied:

$$N_{He}(t) = N_\mu \cdot (E_1 \cdot e^{K_1 \cdot t} \ + \ E_2 \cdot e^{K_2 \cdot t}) \ . \tag{1}$$

Here, $E_1$, $K_1$, $E_2$, $K_2$ are known functions expressed via three rates, $\lambda^{3/2}_{dd\mu}$, $\lambda^{1/2}_{dd\mu}$, $\lambda_{21}$, where the forth rate $\lambda_{12}$ entering the kinetics scheme is determined by the balance equation:

$$\lambda_{12} = \gamma \cdot \lambda_{21}, \quad \gamma = 2 \cdot e^{-\frac{\Delta}{\mathrm{kT}}}, \quad \Delta = 0.0485eV, \quad k = 8.6174 \cdot 10^{-5} eV/K \ . \tag{2}$$

The $^3$He time distributions were fitted with the function $Y(t)=N_{He}(t)+Y_c(t)$, where $Y_c(t)$ is the $\mu$-capture background described above. From these fits, three parameters, $\lambda^{3/2}_{dd\mu}$, $\lambda^{1/2}_{dd\mu}$, $\lambda_{21}$ were determined, (see Tables 1 $\div$ 2 and Fig.3). Qualitatively, the parameters $\lambda^{3/2}_{dd\mu}, \lambda^{1/2}_{dd\mu}, \lambda_{21}$ are determined by the amplitude of the fast exponent at t=0, by the amplitude of the slow exponent at t=0, and by the slope of the fast exponent, respectively. Note that in $D_2$ gas at higher temperature points (300K and 350K) only one exponent was observed in the time distributions of the $^3$He signals. Separation of $\lambda^{3/2}_{dd\mu}$ and $\lambda^{1/2}_{dd\mu}$ in these runs was not possible. It was possible only to determine one parameter, the rate $\lambda_{dd\mu}$ of the dd$\mu$-molecule formation at the steady-state population of the hyperfine states of the d$\mu$-atoms. In Table 1 we present the values of $\lambda^{1/2}_{dd\mu}$ at 300K and 350K recalculated from the measured values of $\lambda_{dd\mu}$, with the values for $\lambda^{3/2}_{dd\mu}$ fixed to

| T K | $\phi$ % | $\lambda^{1/2}_{dd\mu}$ $10^6 s^{-1}$ | $\lambda^{3/2}_{dd\mu}$ $10^6 s^{-1}$ | $\lambda_{21}$ $10^6 s^{-1}$ | R | $\Lambda_Z$ $10^6 s^{-1}$ | $C_Z$ $10^{-6}$ |
|---|---|---|---|---|---|---|---|
| 28.3 | 2.76 | 0.053(3) | 3.98(5) | 37.0(4) | 1.026 | 0.0002 | 0.14 |
| 32.2 | 5.14 | 0.051(1) | 4.13(7) | 37.1(3) | 1.07(3) | 0.003 | 1.2 |
| 36.2 | 5.14 | 0.049(2) | 3.96(6) | 36.6(2) | - | 0.035 | 13.6 |
| 40.3 | 5.14 | 0.050(fix.) | 3.88(6) | 36.6(2) | - | 0.063 | 24.5 |
| 45.3 | 5.05 | 0.0515(8) | 3.92(6) | 36.8(3) | 1.03(3) | 0.0003 | 0.12 |
| 50.2 | 5.13 | 0.0544(fix.) | 3.90(6) | 35.9(3) | - | 0.116 | 45.2 |
| 51.0 | 5.05 | 0.0537(7) | 3.79(4) | 35.77(16) | 1.05(1) | 0.0056 | 2.2 |
| 60.3 | 5.04 | 0.063(1) | 3.89(6) | 36.04(25) | 1.08(2) | 0.00053 | 0.21 |
| 71.0 | 5.04 | 0.088(1) | 4.05(5) | 35.38(25) | 1.24(1) | 0.0054 | 2.2 |
| 96.0 | 5.02 | 0.246(3) | 4.42(7) | 34.8(4) | 1.34(1) | 0.0057 | 2.3 |
| 120.3 | 4.99 | 0.528(4) | 4.98(10) | 35.0(5) | 1.40(1) | 0.0024 | 1.0 |
| 150.3 | 4.97 | 0.943(5) | 5.07(15) | 35.9(9) | 1.43(1) | 0.0034 | 1.4 |
| 200.2 | 4.94 | 1.65(2) | 4.59(15) | 34.2(1.5) | 1.40(1) | 0.004 | 1.6 |
| 250.1 | 4.89 | 2.202(27) | 4.28(12) | 37.0(2.0) | 1.42(1) | 0.007 | 2.9 |
| 300.0 | 4.85 | 2.549(23) | 3.75(fix.) | - | 1.44(1) | 0.012(2) | 4.9 |
| 350.0 | 4.81 | 2.70(5) | 3.28(fix.) | - | 1.44(1) | 0.093(2) | 39.0 |

Table 1

Experimental conditions and results of kinetics fits of the rates of the $\mu$CF processes in pure $D_2$ gas.

the theoretical expectations (solid curves of Fig.3a) using the equation:

$$\lambda_{dd\mu}(\mathrm{T}) = \frac{1}{1+\gamma} \cdot \lambda^{1/2}_{dd\mu}(\mathrm{T}) + \frac{\gamma}{1+\gamma} \cdot \lambda^{3/2}_{dd\mu}(\mathrm{T}) \ . \tag{3}$$

In the $H_2$(50%)+$D_2$(50%) runs, the separation of $\lambda^{3/2}_{dd\mu}$ and $\lambda^{1/2}_{dd\mu}$ was possible even at 300K due to a twofold lower spin-flip rate (Table 2).

The temperature dependence of $\lambda^{3/2}_{dd\mu}(\mathrm{T})$ and $\lambda^{1/2}_{dd\mu}(\mathrm{T})$ (see Fig.3a) demonstrates remarkable resonance behaviour of the dd$\mu$-molecule formation rates. Only at low temperatures T$\leq$ 50K, the dd$\mu$-formation from the F=1/2 d$\mu$-state is non-resonant. The non-resonant mechanism gives the main contribution to the dd$\mu$-formation on the HD molecules in the whole investigated temperature range. The HD runs were performed with the goal to study the non-resonant dd$\mu$-formation process, while resonant one is suppressed. The main problem of this experiment was elimination of $D_2$ from the HD gas as the dd$\mu$ formation rate on $D_2$ is by a factor of 20 larger than on HD (at T=300K). Using a specially developed method [13], we prepared very clean HD gas containing only $\sim 1\%$ of $D_2$ molecules. Still the background due to dd-fusion on $D_2$ molecules was con-

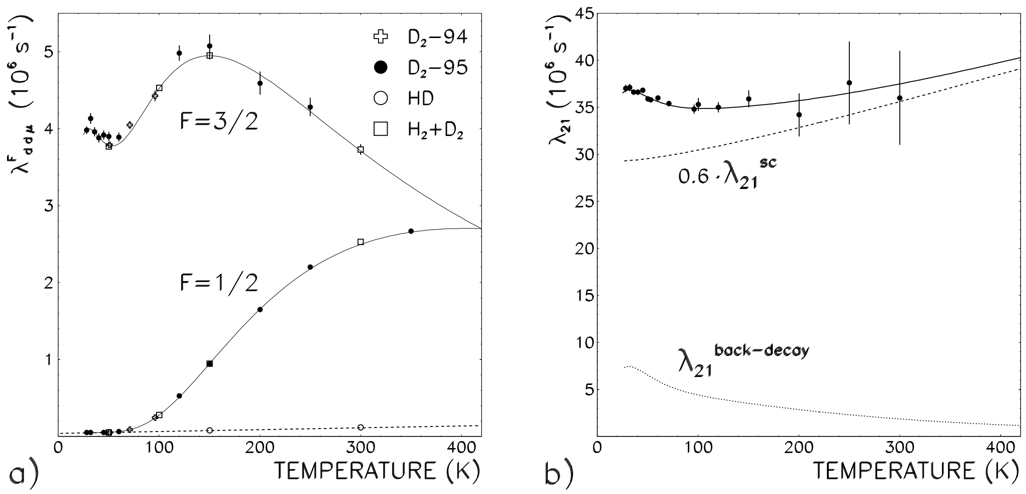


Figure 3. a) Absolute rates for $dd\mu$ formation versus temperature in $D_2$ and in H/D gas mixtures. The curves present the fit by the theory. b) Spin-flip rates on $D_2$ molecules. Full curve: fit of the experimental data by superposition of the two theoretical curves (dashed and dotted lines) after renormalisation of the non-resonant curve.

siderable. It was separated by observing the fast exponent in the time spectra. In this way, the $C_{D_2}$ concentration was determined, and it proved to be in good agreement with the chromothographic analysis of the gas (Table 3).

In the fits of the $^3$He time distributions, we assumed that the rates of the dd$\mu$ formation on HD $\lambda_{dd\mu}^{HD}$ are equal for both d$\mu$ spin states. The results of the fits are presented in Table 3 and in Fig.3a. The observed distribution $\lambda_{dd\mu}^{HD}(\mathrm{T})$ shows a weak linear dependence with temperature:

$$\lambda_{dd\mu}^{HD}(\mathrm{T}) = (2.4 \cdot 10^{-4} \cdot \mathrm{T} + 0.041)\ \mu s^{-1}\ . \tag{4}$$

Such a dependence is in qualitative agreement with the theoretical prediction for non-resonant dd$\mu$ formation rates [14]:

$$\lambda_{dd\mu}^{\mathrm{nr}}(\mathrm{T}) = 2.4 \cdot 10^{-4} \cdot \mathrm{T} + 0.027 \tag{5}$$

## *2.2. Temperature dependence of the spin-flip rate $\lambda_{21}(T)$*

The d$\mu$ spin-flip rate contains two components. One is direct spin transfer $(d\mu)_{F=3/2} \rightarrow (d\mu)_{F=1/2}$ in the non-resonant scattering of the d$\mu$ atoms on $D_2$

| T<br>K | gas mixture<br>state | $\phi$<br>% | $\lambda_{dd\mu}^{1/2}$<br>$10^6 s^{-1}$ | $\lambda_{dd\mu}^{3/2}$<br>$10^6 s^{-1}$ | $\lambda_{21}$<br>$10^6 s^{-1}$ | $\Lambda_Z$<br>$10^6 s^{-1}$ | $C_Z$<br>$10^{-6}$ |
|---|---|---|---|---|---|---|---|
| 50 | EQ | 5.07 | 0.058(4) | 3.66(3) | 34.0(4) | 0.0032(6) | 1.3 |
| 50 | NE | 5.12 | 0.051(4) | 3.74(3) | 35.5(3) | 0.0053(6) | 2.1 |
| 100 | EQ | 5.00 | 0.279(8) | 4.50(5) | 33.9(5) | 0.0035(10) | 1.4 |
| 150 | EQ | 4.97 | 0.95(1) | 4.88(5) | 35.6(7) | 0.0036(6) | 1.4 |
| 150 | NE | 5.02 | 0.934(10) | 4.94(6) | 35.5(7) | 0.004(1) | 1.5 |
| 300 | EQ | 4.91 | 2.55(6) | 3.62(18) | 52(10) | 0.0043(9) | 1.6 |
| 300 | NE | 4.97 | 2.51(3) | 3.70(7) | 35(5) | 0.0040(10) | 1.5 |

Table 2

Experimental conditions and results of kinetics fits of the rates of $\mu$CF processes in $H_2$(50%)+$D_2$(50%) gas mixture. EQ - equilibrium and NE - non equilibrium mixtures.

| T<br>K | $\phi$<br>% | $\lambda_{dd\mu}^{HD}$<br>$10^6 s^{-1}$ | R | $C_{D2}$<br>% | $C_{D2}^{\mathrm{chr}}$<br>% | $\Lambda_Z$<br>$10^6 s^{-1}$ | $C_Z$<br>$10^{-6}$ |
|---|---|---|---|---|---|---|---|
| 50 | 4.74 | 0.0561(8) | 0.99(2) | 1.16(3) | 1.10 | 0.0043 | 1.7 |
| 150 | 4.78 | 0.0801(24) | 1.01(2) | 1.06(5) | 1.02 | 0.0027 | 1.3 |
| 300 | 4.87 | 0.119(6) | 1.00(2) | 0.82(8) | 0.78 | 0.0032 | 1.5 |

Table 3

Experimental conditions and results of kinetics fits of the rates of $\mu$CF processes in HD gas. $C_{D2}$ and $C_{D2}^{\mathrm{chr}}$ are the values of the concentrations of $D_2$ molecules obtained by fit of $^3$He time distributions and by chromotographic analysis, respectively.

molecules with the rate $\lambda_{21}^{\mathrm{sc}}(\mathrm{T})$. The second one is the contribution $\lambda_{21}^{\mathrm{bd}}(\mathrm{T})$ to spin-flip via back-decay of the dd$\mu$-molecule. The theory [21,16] predicts significantly different shapes of the temperature dependences of these two rates (Fig.3b) allowing to separate the two components in fitting to the measured $\lambda_{21}(\mathrm{T})$ by the sum:

$$\lambda_{21}(\mathrm{T}) = \alpha \cdot \lambda_{21}^{\mathrm{bd}}(\mathrm{T}) + \beta \cdot \lambda_{21}^{\mathrm{sc}}(\mathrm{T}) \ . \tag{6}$$

Here $\alpha$ and $\beta$ are the normalization factors to be found from the fit, the temperature dependences of the two components being taken from the theory. This procedure can reproduce the experimental data on $\lambda_{21}(\mathrm{T})$ (see Fig.3b) only when the theoretical function $\lambda_{21}^{\mathrm{sc}}(\mathrm{T})$ is renomalized by a factor 0.6, while the back-decay rate can be kept close to the theoretical prediction ($\alpha \approx 1$). The disagreement with the theory of $\lambda_{21}^{\mathrm{sc}}(\mathrm{T})$ is unclear and needs theoretical explanation.

| $R_{J=0}$ | $R_{J=1}$ | Comments |
|---|---|---|
| 0.886 | 1.43 | Coulomb-corrected R-matrix calculation [18] |
| 0.902(5) | 1.459(16) | phase-shift analysis of the exp. data [17] |
| 0.901(12) | 1.450(11) | direct measurement (this work) |

Table 4
World results of measured *dd* fusion branching ratios.

*2.3. Branching ratio of dd-fusion channels*

The branching ratio of the dd-fusion channels, R=N($^3$He+n)/N(t+p), was measured in the $D_2$ and HD runs using the amplitude distribution for the steady state region (Fig.2a). It was determined by the ratio of the number of events in the energy range $(0.45 \div 0.90)$MeV to that in the energy range $(0.90 \div 4.0)$MeV. Only one correction for the pileup of the next fusion on the $^3$He signal was applied. As a result, the ratio R was determined with a precision of $1 \div 3\%$. The results are presented in Tables 1 and 3 and in Fig.4a. In the case of d-$\mu$-d fusion in $D_2$ gas, a strong temperature dependence of R(T) is seen. On the other hand, R(T)$\sim$constant in the case of d-$\mu$-d fusion in the HD gas. The following expression was used to fit the experimental points:

$$\mathrm{R(T)} = \frac{(\lambda_{dd\mu}(\mathrm{T}) - \lambda_{dd\mu}^{\mathrm{nr},J=0}(\mathrm{T}))\cdot \mathrm{R}_{J=1} + \lambda_{dd\mu}^{\mathrm{nr},J=0}(\mathrm{T})\cdot \mathrm{R}_{J=0}}{\lambda_{dd\mu}(\mathrm{T})}\ . \tag{7}$$

Here, $J$ is a total orbital momentum of dd$\mu$ molecule, $R_{J=1}$ and $R_{J=0}$ are free parameters, $\lambda_{dd\mu}(\mathrm{T})$ is the steady state dd$\mu$ formation rate determined by equation (3), $\lambda_{dd\mu}^{\mathrm{nr},J=0}(\mathrm{T}) = \lambda_{dd\mu}^{HD}(\mathrm{exp}) - \lambda_{dd\mu}^{\mathrm{nr},J=1}(\mathrm{theor})$ where $\lambda_{dd\mu}^{\mathrm{nr},J=1}(\mathrm{theor}) = 0.012\mu s^{-1}$ [14]. The fit results are presented in Table 4. Strong isotopic asymmetry of dd-fusion is seen in the $J=1$ dd$\mu$-state where the fusion occurs in the P-wave of the dd-system. Similar effect was observed in the phase-shift analysis of the dd-scattering data [17]. Recently, this asymmetry was reproduced by a theory based on the Coulomb-corrected R-matrix calculations [18].

*2.4. Muon sticking probability*

The effective muon sticking probability $\omega_d$ was determined from the ratio of the number of events in the $^3$He$\mu$ peak to that in the $^3$He and $^3$He$\mu$ peaks in the amplitude distribution of the dd-fusion signals: $\omega_d$ =N($^3$He$\mu$)/N($^3$He+$^3$He$\mu$). To determine N($^3$He$\mu$), an additional amplitude spectrum was compiled with the requirement of the first fusion followed by a second one ("survived muon method"

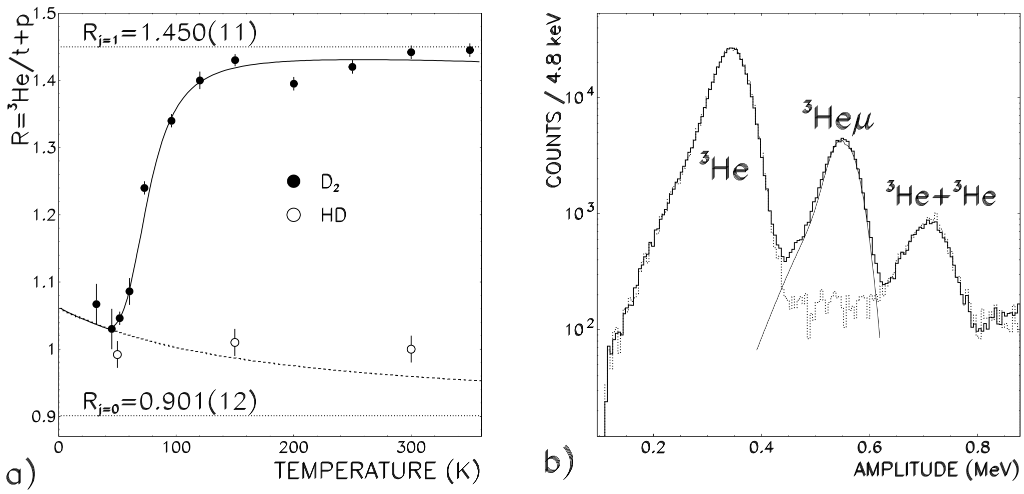


Figure 4. a) dd-fusion branching ratio R=N($^3$He+n)/N(t+p) in $D_2$ and in HD gases, plotted versus gas temperature. The lines are the results of the fit with equation (6). The dashed line corresponds to R(T) of the non-resonant dd$\mu$ formation. b) Amplitude spectra of fusion signals from the IC at T=300K and $\phi = 0.0837$ in pure deuterium corresponding to the $^3$He channel. The dotted line shows the spectrum evaluated by the "survived muon method", where sticking events are absent. The remained spectrum in this region consists mainly of stripped events where the muon was shaken off from $^3$He$\mu$ [19].

[6]). This spectrum, normalized to the $^3$He peak, is presented in Fig.4b by the dotted line. The difference between these two spectra in the region of the $^3$He$\mu$ peak gives the number N($^3$He$\mu$) with high precision. Only one small correction for the pileup of the next fusion on the $^3$He signal was applied. The results of the measurements at two deuterium densities are:

$$\omega_d(\phi = 0.0837) = 0.1206(6); \qquad \omega_d(\phi = 0.0485) = 0.1205(7)$$

with mainly statistical errors. These results can be compared with the recent theoretical calculations: $\omega_d^{th} = 0.122$ [20].

## 3. Comparison of the measured rates with $\mu$CF theory

The temperature dependences $\lambda^{3/2}_{dd\mu}$(T), $\lambda^{1/2}_{dd\mu}$(T), and $\lambda_{21}$(T) presented above were fitted by the theoretical distributions [15,21] simultaneously, with a set of basic theoretical parameters left free in the fit. The comparison of the obtained by such way parameters with the theoretical values is a sensitive test of the $\mu$CF

| Parameter | Fit value | Theory | Comments |
|---|---|---|---|
| $\epsilon_{11}$ | -1.9626(3) | -1.9648 (eV) | the loosely bound energy level in dd$\mu$ molecule [4] |
| $\lambda_f^{J=1}$ | 407(20) | 460 ($10^6$s$^{-1}$) | the effective dd fusion rate in $(\mathrm{dd}\mu)_{J=1,\nu=1}$ state [15,22] |
| $C_{\Delta F}$ | 1.021(3) | 1.00 | s.f. for d$\mu$ hfs splitting energy [23] |
| $C_{\Delta S}$ | 0.999(9) | 1.00 | s.f. for the dd$\mu$ hfs splitting energy [23] |
| $C_{KI}$ | 1.01(6) | 1.00 | s.f. of the rotational energy levels for the $D_2$ molecule [24] |
| $C_{KF}$ | 0.754(60) | 1.00 | s.f. of rotational energy levels for the $[(dd\mu)dee]$ complex [24] |
| $C_{\mathrm{matr}}$ | 0.746(20) | 1.00 | s.f. of matrix elements [15,21] |
| $\beta$ | 0.60(1) | 1.00 | s.f. of non-resonant spin-flip rate [16] |

Table 5
Fit values of theoretical parameters extracted from the measured rates $\lambda^{3/2}_{dd\mu}$(T), $\lambda^{1/2}_{dd\mu}$(T), and $\lambda_{21}$(T). "s.f." means scaling factor.

theory. Table 5 demonstrates such a comparison. One can see from Fig.3a the very good quality of the fit. In particular, this fit allowed to extract the energy $\varepsilon_{11}$ of the loosely bound level in the dd$\mu$-molecule with precision of $\pm 0.3$ meV. This value is only by 2 meV different from the theoretical value. Note that even vacuum polarization contribution to $\varepsilon_{11}$ is about 10 meV. The other parameters listed in Table 5 proved to be also close to the theoretical values except some renormalization needed for $\lambda^{\mathrm{SC}}_{21}$(T), parameter $\beta$.

## 4. Summary

The new experimental method developed originally at PNPI, the high pressure hydrogen time projection chamber, combined with the unique quality of the $\mu$E4 muon beam at PSI, allowed to carry out detailed study of muon catalyzed dd-fusion in $D_2$, $H_2$+$D_2$, and HD gas. The main parameters of the $\mu$CF processes for d-$\mu$-d have been measured in a wide temperature range from T=28K to T=350K with high absolute precision, namely: resonant and non-resonant dd$\mu$ - molecule formation rates; direct and back-decay spin-flip rates in the d$\mu$-atom; branching ratios of the dd-fusion channels; muon sticking probability.

The resulting data were analyzed using the $\mu$CF theory that allowed to check several most important theoretical parameters. In particular, the energy $\varepsilon_{11}$ of the losely bound level in the dd$\mu$-molecule was determined with unprecedent absolute accuracy of $\pm 0.3$ meV. The general agreement of the experiment with the theory was found to be good, with only one exception: the experimental direct spin-flip rate $\lambda^{\mathrm{SC}}_{21}$(T) is significantly lower than the theoretical prediction.

**Acknowledgements**
This work was supported in part by the Russian Foundation of Fundamental Research, grant № 00 − 15 − 96813, by the Russian Ministry of Sciences and Technology, and by the Paul Scherrer Institute. Authors thank Prof. L.I. Ponomarev for permanent interest to this work and discussions.

## References

[1] V.P. Dzhelepov et al., Soviet. Phys. JETP **19** (1964) 1376 and 23 (1966) 820.
[2] E.A. Vesman, Soviet. Phys. JETP **5** (1967) 9.
[3] W.H. Breunlich, et al., Ann. Rev. Nucl. Part. Sci **39** (1989) 311; L.I. Ponomarev, Contemp. Phys. **31** (1991) 219; C. Petitjean, Nuclear Phys. **A 543** (1992) 79; P. Kammel, Muonic Atoms and Molecules, eds. L. Schaller and C. Petitjean (Birkhäuser, Basel, 1993) 111.
[4] L.I. Ponomarev, this procceding.
[5] A. Scrinzi et al., Phys. Rev. **A 47** (1993) 4691.
[6] D.V. Balin et al., MCF **7** (1992) 1.
[7] C. Petitjean et al., Hyp. Interact. **101/102** (1996) 1.
[8] G.G. Semenchuk et al., Hyp. Interact. **101/102** (1996) 547.
[9] P. Ackerbauer et al., Phys. Lett. **B 417** (1998) 224;
N.I. Voropaev et al., Thesis (Russia PNPI Gatchina, 1998).
[10] C. Petitjean et al., Hyp. Interact. **118** (1999) 127.
[11] N.I. Voropaev et al., Hyp. Interact. **118** (1999) 135.
[12] G.G. Semenchuk et al., Hyp. Interact. **118** (1999) 141.
[13] G.N. Schapkin et al., preprint PNPI-2395, RAN, Gatchina 2000.
[14] M.P. Faifman, MCF **4** (1989) 341.
[15] L.I. Men'shikov et al., Sov. Phys. JETP **65** (1987) 656.
[16] A.Adamczak et al., Atomic Data and Nuclear Data Tables, **Vol.62**, **No.2**, (1996) 315,329.
[17] B.P. Adyasevich, V.G. Antonenko and D.E. Fomenko, Yad.Fiz. **33** (1981) 1167.
[18] G.M. Hale, Muon Cat. Fusion **5/6** (1990/91) 227.
[19] T. Case et al., Hyp. Interact. **118** (1999) 197.
[20] L.I. Men'shikov and L.I. Ponomarev, JETP Lett. **41** (1985) 623.
[21] M.P. Faifman, L.I. Men'shikov and T.A. Strizh, MCF **4** (1988) 1; M.P. Faifman et al., Hyp. Interact. **101/102** (1996) 179.
[22] L.N. Bogdanova et al., Phys. Lett. **115B** (1982) 171; Errata **167B** (1986) 485;
[23] D. Bakalov MCF **3** (1988) 321.
[24] M.P. Faifman et al., Z. Phys. **D2** (1986) 79.